Appl. Phys. A (2015) 120:341–347
DOI 10.1007/s00339-015-9192-2

Applied Physics A
Materials Science & Processing

Room-temperature embedment of anatase titania nanoparticles into porous cellulose aerogels

Yue Jiao[1] · Caichao Wan[1] · Jian Li[1]

Received: 10 January 2015 / Accepted: 20 April 2015 / Published online: 29 April 2015

Abstract In this paper, a facile easy method for room-temperature embedment of anatase titania (TiO_2) nanoparticles into porous cellulose aerogels was reported. The obtained anatase TiO_2/cellulose (ATC) aerogels were characterized by scanning electron microscopy, energy-dispersive X-ray spectrometer, transmission electron microscopy, X-ray photoelectron spectroscopy, X-ray diffraction, nitrogen adsorption measurements, and thermogravimetric analysis. The results showed that high-purity anatase TiO_2 nanoparticles with sizes of 3.69 ± 0.77 nm were evenly dispersed in the cellulose aerogels, which leaded to the significant improvement in specific surface area and pore volume of ATC aerogels. Meanwhile, the hybrid ATC aerogels also had a high loading content of TiO_2 (ca. 17.7 %). Furthermore, through a simple photocatalytic degradation test of indigo carmine dye under UV light, ATC aerogels exhibited superior photocatalytic activity and shape stability, which might be useful in some fields like governance of water pollution, and chemical leaks.

1 Introduction

Organic/inorganic hybrid materials have emerged as quite intriguing materials, due to their combining organic and inorganic materials' superb characters, which hold great potential in many applications such as adsorbents, catalysts, fuel cells, and sensors [1–4]. Among various natural organic polymers, undoubtedly, cellulose is high profile; this kind of unbranched polymer of β-1, 4-linked glucopyranose is acclaimed and has been extensively applied in every walk of life such as papermaking, adhesive, architectural coating, and biomedicine. However, it is difficult for cellulose to be dissolved, hydrolyzed, and processed in some common aqueous or organic solvents, owing to its some inherent structure features such as strong inter- and intra-molecular hydrogen bonds, high degree of polymerization, and high degrees of crystallinity [5]. In recent decades, some effective cellulose solvents were successively reported [6–9], contributing to further exploiting and fabricating novel cellulose products (such as films, foams, and aerogels). As one of the most promising cellulose products, cellulose aerogels consist of cross-linked three-dimensional (3D) network. The unique structural characteristic endows themselves with low density, high porosity, and large specific surface area. As a result, cellulose aerogels may find applications in multitudinous fields such as adsorbing materials, catalyst supports, super-thermal and sound insulators, and electronic devices [10–12]. In particular, cellulose aerogels are also extremely promising matrix materials in the domain of nanocomposites synthesis. Their hierarchical micro- and nanoporous structures are beneficial to achieve controlled growth of nanoparticles; besides, abundant surface hydroxyl groups of cellulose are also suitable binders for immobilization of nanoparticles in the matrix [13]. In recent years, plentiful investigations have been undertaken extensively for organic/inorganic hybrid materials using cellulose aerogels as matrixes [14–16]. The synthetic composites exhibit numerous attractive performances including photocatalytic ability, antibacterial

Yue Jiao and Caichao Wan have contributed equally to this work and are considered co-first authors.

✉ Jian Li
lijiangroup@163.com

[1] Material Science and Engineering College, Northeast Forestry University, No. 26, Hexing Road Xiangfang District, Harbin 150040, People's Republic of China

property, high mechanical strength, and magnetic property.

Titania (TiO_2) nanoparticles are one of the most noticeable inorganic nanoparticles at present, which could be served as solar cells, photocatalyst for air and water purification, high permittivity dielectric layers for electronic devices, sensors for gas and biomolecules, and biocompatible coatings for biomaterial petroleum processing [17]. In nature, TiO_2 mainly occurs in four distinct crystallographic phases: anatase (tetragonal, space group $I4_1/amd$), rutile (tetragonal, space group $P4_2/mnm$), brookite (orthorhombic, space group P*bca*), and TiO_2 (B) (monoclinic, space group $C2/m$) [18]. Meanwhile, anatase TiO_2 phase is wildly believed to have more superior photocatalytic activity within these four kinds of polymorphs [19], which is more dominant in some applications such as photodecomposition and solar energy conversion. However, owing to some intractable problems like difficultly recycling TiO_2 powders from treated aqueous solutions, nano-TiO_2 is still limited to small-scale applications. Consequently, nanocomposites that combine nano-TiO_2 with some special substrates with large specific surface area (such as cellulose aerogels) have attracted increasing attention [20, 21]. Taking examples of cellulose aerogels, embedding anatase TiO_2 nanoparticles into nanoporous cellulose aerogels might contribute to not only guiding growth of the nanoparticles, but also inhibiting spontaneous agglomeration of nanoparticles caused by high surface energy and chemical activity of nanoparticles. Besides, anatase TiO_2/cellulose (ATC) aerogels composites probably inherit various functions from the individual components such as photocatalytic property, bacteriostatic activity, and strong adsorption capacity. This multifunctional feature makes ATC aerogels applied to a wider range of occasions.

In general, anatase TiO_2 phase could be prepared by multiple methods such as sol–gel technique, calcination, hydrothermal method, chemical vapor deposition, and thermal hydrolysis [22–26]. In continuation of environmentally benign and low energy consumption methods for synthesis of nanoparticles, herein, we reported a mild and effective method to fabricate anatase TiO_2 nanoparticles that were embedded in porous cellulose aerogels at room temperature by simply immersing cellulose hydrogels in an anatase TiO_2 nanosol. Meanwhile, a green cost-effective NaOH/polyethylene glycol (PEG) aqueous solution was carried out to fabricate cellulose hydrogels (the precursor of cellulose aerogels). Moreover, an easy photocatalytic degradation experiment for ATC aerogels was performed under UV light to roughly demonstrate the photochemical utilization potentiality.

2 Materials and methods

2.1 Materials

All reagents were commercially available and of reagent grade. Cellulose was isolated from waste wheat straw by chemical pretreatment, and the pretreatment process could refer to our previous reports [27]. The purified cellulose was dried at 60 °C for 24 h before used. Deionized water was used for all experiments.

2.2 Preparation of anatase TiO_2 nanosol

Anatase TiO_2 nanosol was fabricated according to the method reported by Wu et al. [28]. Briefly, absolute ethyl alcohol (20 mL) and tetrabutyl titanate (5 mL) were firstly mixed homogeneously with magnetic stirring for 30 min at room temperature, and then the obtained mixed solution was added dropwise into 0.04 M HNO_3 solution (200 mL) at room temperature with continuous magnetic stirring. After that, the mixture was kept stirring for 48 h to ensure complete hydrolysis, nucleation, and growth of TiO_2 crystallites. Finally, the mixed solution was stirred for another 48 h, and the following pale blue anatase TiO_2 nanosol was obtained. During this 96-h stirring, it could be seen that the previous emulsion was significantly transformed to a transparent solution. Moreover, the sol could be stably kept at room temperature for several months without sedimentation or delamination.

2.3 Preparation of anatase TiO_2/cellulose aerogel

The desired amount of cellulose was added to a mixed aqueous solution of NaOH/PEG-4000 at a mass ratio of 9/1 with magnetic stirring for 5 h at room temperature to form a homogeneous cellulose solution with 2 % concentration. Then, the cellulose solution was frozen for 12 h at −15 °C and subsequently thawed at ambient temperature with vigorous stirring for 30 min. After being frozen again for 5 h at −15 °C, the solution was placed into a 1 % HCl coagulating bath for 6 h, repeating this impregnation process until the formation of a white hydrogel. Thereafter, the hydrogel was repeatedly rinsed with a good deal of distilled water, and the obtained clean cellulose hydrogel was immediately immersed in the above-mentioned anatase TiO_2 nanosol for 3 h at room temperature. After the immersion treatment, the obtained ATC hydrogel was heated at 60 °C for 5 min in a thermostatic water bath and subsequently cured at 100 °C for 5 min to complete the formation of nano-TiO_2 in the pore structure of cellulose hydrogel. Finally, ATC hydrogel was washed several times by distilled

water and tert-butyl alcohol in sequence to remove unattached TiO_2 particles and other residual chemicals and then subjected to a freeze-drying process for 48 h at −30 °C in vacuum, and the following ATC aerogel was fabricated. In addition, the pure cellulose (PC) aerogel was prepared by direct tert-butyl alcohol freeze-drying treatment of cellulose hydrogel without the above-mentioned immersion process. The anatase TiO_2 particles were obtained by the drying treatment of the nanosol in a vacuum oven at 60 °C for 48 h.

2.4 Indigo carmine dye photocatalytic degradation

The photocatalytic activity of ATC aerogels was roughly evaluated by observing the changes in color during the photocatalytic degradation process of indigo carmine dye. The indigo carmine dye (50 mL, 5×10^{-5} mol L^{-1}) and ATC aerogels sample with sizes of about 30 mm (diameter) × 15 mm (height) (ca. 0.79 g) were put into a clean glass dish and then stirred in the dark for 30 min to achieve adsorption equilibrium. Thereafter, the dish was placed in a closed chamber with a UV source (mercury lamp, 120 W, and 365 nm). The distance between the UV source and the dish was around 10 cm. The dish was exposed to the mercury lamp for about 1 h, monitoring the color changes during the entire photocatalytic degradation process.

2.5 Characterizations

Microstructures and surface chemical compositions were determined by scanning electron microscopy (SEM, FEI, and Quanta 200) equipped with an energy-dispersive X-ray spectrometer (EDXS). Transmission electron microscopy (TEM) observations were carried out on a FEI, Tecnai G2 F20 TEM. X-ray photoelectron spectra (XPS) were recorded in the range of 0–1400 eV using Thermo ESCALAB 250Xi XPS spectrometer (Germany). Crystal structures were characterized via X-ray diffraction (XRD, Rigaku, and D/MAX, 2200) operating with Cu Kα radiation ($\lambda = 1.5418$ Å) at a scan rate (2θ) of 4° min^{-1} ranging from 5° to 70°. Nitrogen adsorption measurements were taken with an accelerated surface area and porosimetry system (3H-2000PS2 unit, Beishide Instrument S&T Co., Ltd). Brunauer–Emmett–Teller (BET) analysis was carried out for a relative vapor pressure of 0.05–0.3. Barrett–Joyner–Halenda (BJH) analysis was performed for desorption branch. Thermogravimetric analysis (TGA) was performed with a synchronous thermal analyzer (the USA, SDT-Q600) from room temperature to 800 °C at a heating rate of 10 °C min^{-1} under a nitrogen atmosphere.

3 Results and discussion

The SEM image in Fig. 1a demonstrated that ATC aerogels maintained interconnected 3D network after the immersion and heating processes. Moreover, the 3D architecture was possibly generated by self-assembly of cellulose chains due to large-scale hydrogen bond connection as the result of the plentiful surface hydroxide radicals [29]. However, it is hard to distinguish the synthetic nanoparticles from the complicated network structure. Even higher magnification SEM image (50,000 times) still could not clearly identify the nanoparticles (Fig. 1b), possibly due to their extremely small particle size, and the following TEM observation would prove that. In addition, compared with PC aerogels, apart from the common C and O elements, the EDX spectrum of ATC aerogels exhibited new strong peak assigned to Ti element (inset in Fig. 1b), which indicated the presence of plentiful titanium compound. Furthermore, the dramatic decline in the atomic ratio of C/O from 1.12 to 0.83 was another potential evidence of the presence of titanium oxide.

It is of note that the properties of nanocomposites are tightly associated with the diameters and dispersion of nanoparticles in matrixes [30, 31]. According to the TEM observation (Fig. 2a, b), the formed nanoparticles were homogeneously dispersed and immobilized in cellulose aerogel matrixes as indicated by the dark spots, and no severe agglomeration phenomena occurred, which

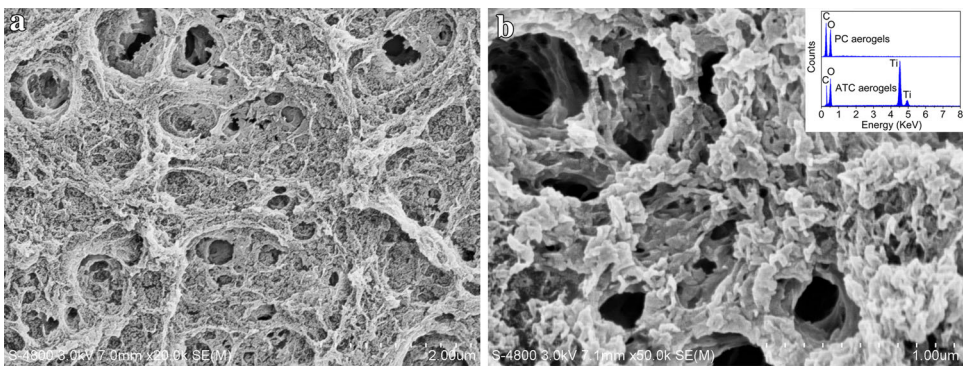

Fig. 1 **a**, **b** SEM images of different magnification of ATC aerogels. The *inset* in **b** exhibited the corresponding EDX spectra of PC aerogels and ATC aerogels

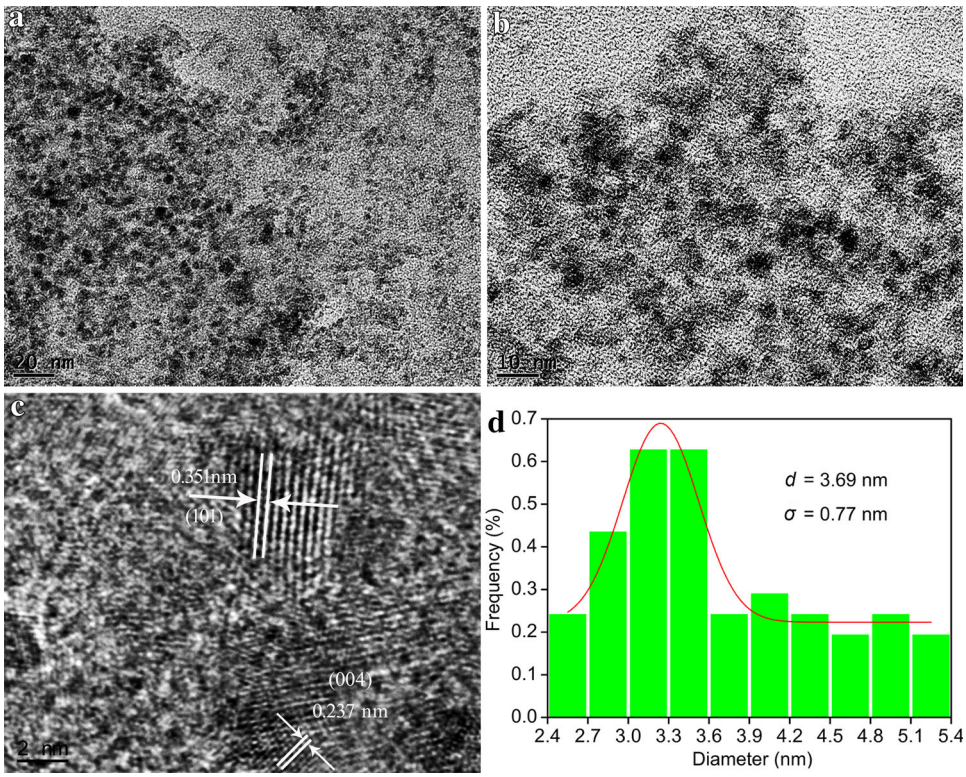

Fig. 2 **a**, **b** TEM images of different magnification and **c** HRTEM image of ATC aerogels. **d** Size distribution of the TiO_2 nanoparticles in the cellulose aerogels

indicated that the 3D architecture of porous cellulose aerogels might be a suitable template for the synthesis of nanoparticles. Meanwhile, this class of matrix materials might also be expanded to fabricate other versatile oxide nanoparticles/cellulose aerogels composites. High-resolution transmission electron microscopy image demonstrated the presence of anatase TiO_2 as shown in Fig. 2c; i.e., lattice fringes with a spacing of 0.351 and 0.237 agreed well with the (101) and (004) planes of anatase TiO_2 [32]. Moreover, the particle size distribution that was calculated based on the TEM images is shown in Fig. 2d. The results showed that the diameter histogram exhibited Gaussian-like distributions, and the synthetic nanoparticles were polydisperse. Their mean diameter (d) and standard deviation (σ) were estimated to be 3.69 and 0.77 nm, respectively.

Figure 3a showed survey scan XPS spectrum of ATC aerogels, and the spectrum clearly revealed that the main elements on the sample surface were Ti, O, and C. Figure 3b presented the Ti ($2p_{3/2}$, $2p_{1/2}$) spectra. The binding energies of Ti $2p_{3/2}$ and Ti $2p_{1/2}$ were 458.6 and 464.4 eV, respectively, indicating the typical presence of Ti^{4+} (TiO_2) [33, 34]. Figure 3c displayed the O1s spectra. The O1s peak at 530.0 eV was corresponding to lattice oxygen of Ti^{4+}–O, while the higher binding energy of 532.8 eV was assigned to hydroxyl groups (O–H) [35], respectively. Figure 4d showed the C1s spectra. Three peaks were observed after multi-peak Gaussian fitting. The peak located at 284.8 eV was ascribed to carbon atoms in C–C, C=C, and C–H bonds. The peak at 286.4 eV was assigned to the C–O bond, and the peak at 287.8 eV was attributed to the C=O bond [36]. Therefore, the XPS results further confirmed the formation of TiO_2 via the aforementioned preparation approach.

To determine the crystal phase of the formed TiO_2 particles, XRD measurements were taken. Deconvolution of the overlapping peaks was performed using a mixed Gaussian–Lorentzian fit program. As shown in Fig. 4, the pattern of the synthetic TiO_2 nanoparticles showed the presence of peaks ($2\theta = 25.14°$, 37.64°, 47.78°, 54.14°, 55.62°, 62.76°, and 68.96°) assigned to anatase-type TiO_2 (JCPDS, 21-1272) [37], and no excess peaks related to rutile or brookite TiO_2 were detected, implying that only high-purity anatase TiO_2 nanoparticles were formed via the mild room-temperature synthesis method. Compared with the TiO_2 nanoparticles, the new diffraction peaks ($2\theta = 12.56°$, 20.20°, and 21.68°) as shown in the pattern of ATC aerogels were originated from the (101), ($10\bar{1}$), and (002) planes of cellulose II crystal structure, corresponding to the characteristics of the cellulose aerogel matrixes [38]. In addition, some peaks belonging to anatase TiO_2 could also be clearly distinguished at around 25.58°, 37.80°, 47.97°, 54.15°, 55.65°, 63.18°, and 68.86°, demonstrating that the anatase TiO_2 nanoparticles were successfully embedded into the porous cellulose aerogel matrixes.

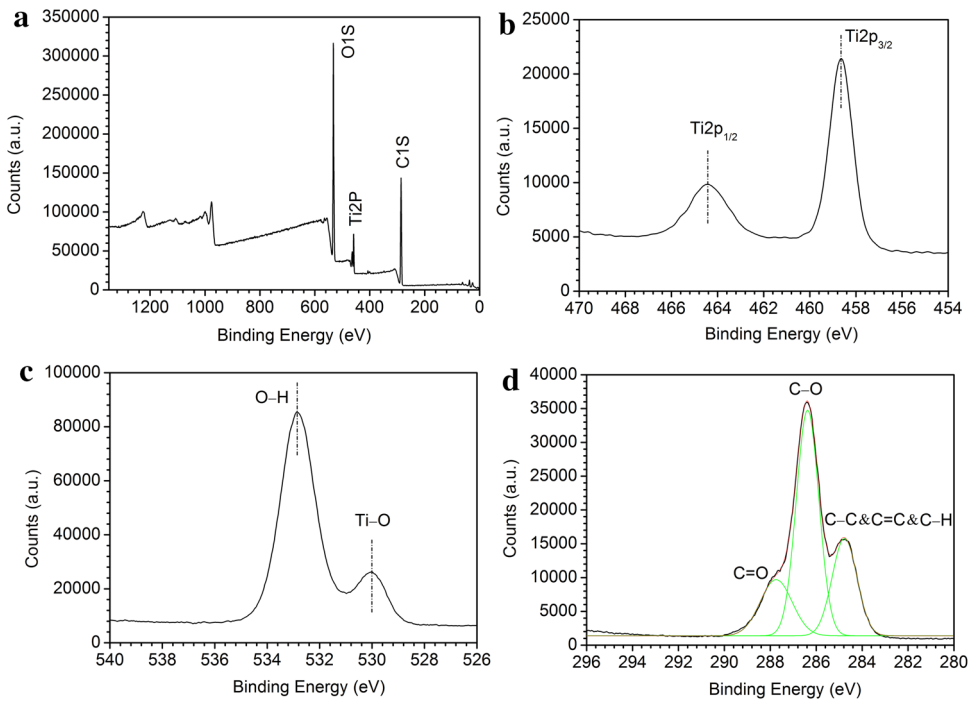

Fig. 3 **a** Survey scan, **b** Ti 2p, **c** O1s, and **d** C1s XPS spectra of ATC aerogels, respectively

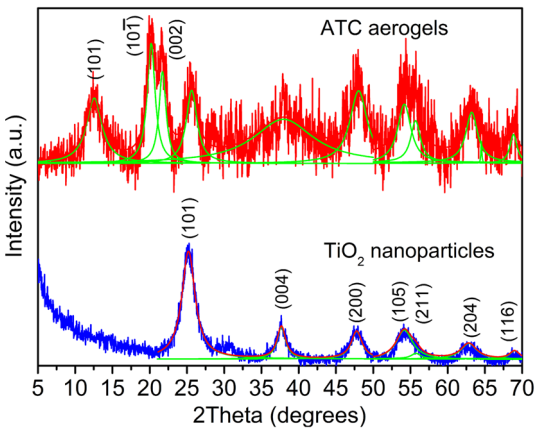

Fig. 4 XRD patterns of ATC aerogels and the TiO_2 nanoparticles, respectively

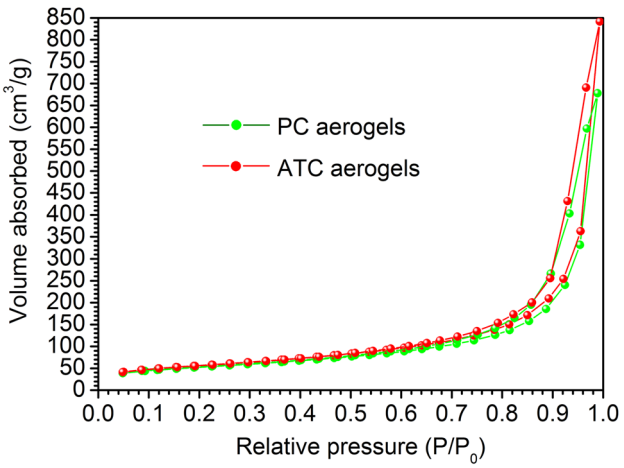

Fig. 5 Nitrogen adsorption and desorption isotherms of PC aerogels and ATC aerogels, respectively

Nitrogen adsorption measurements were used to estimate specific surface area and porosity characteristics of PC aerogels and ATC aerogels, and the corresponding sorption isotherms are shown in Fig. 5. According to the IUPAC classification, the both sorption isotherms were of type IV [39]. At low relative pressure, the adsorption uptakes of the samples increased slowly, and nitrogen molecules were gradually adsorbed on the internal surface of porous structures from single to multilayer. In addition, the samples showed the isotherms with clear upward deviations (P/P_0 at 0.6–0.9) which was caused by capillary condensation, suggesting the characteristic of mesoporous structure. Furthermore, the larger amount of adsorption (without apparent limitation) occurring at relative pressures above 0.9 demonstrated the presence of macropores. The hysteresis loops for the both samples were of type H3 without obvious adsorption limits at P/P_0 close to 1, possibly revealed the existence of slit-shaped pores [40]. Specific surface area and pore volume are two important structural characteristics of aerogels, and high values are desirable for applications such as functional carriers and adsorbing materials. The BET analysis of PC aerogels and ATC aerogels gave specific surface areas of around 185 and 201 $m^2\ g^{-1}$, respectively. The mesopore analysis by BJH method gave pore volumes of approximately 1.0 and

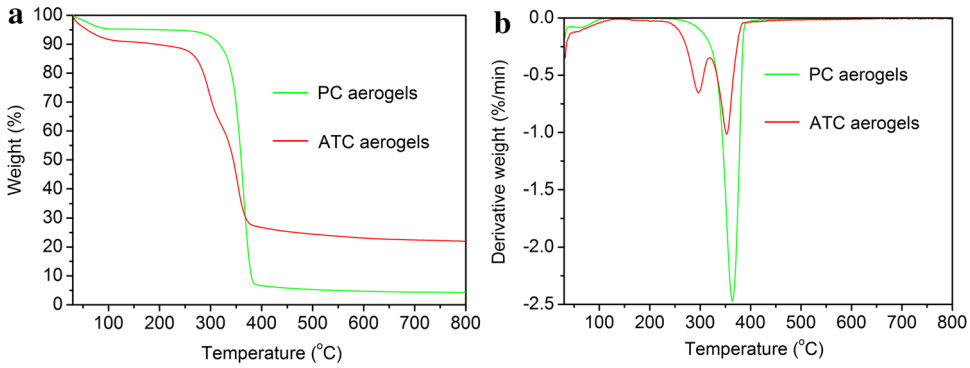

Fig. 6 **a** TG and **b** DTG curves of PC aerogels and ATC aerogels, respectively

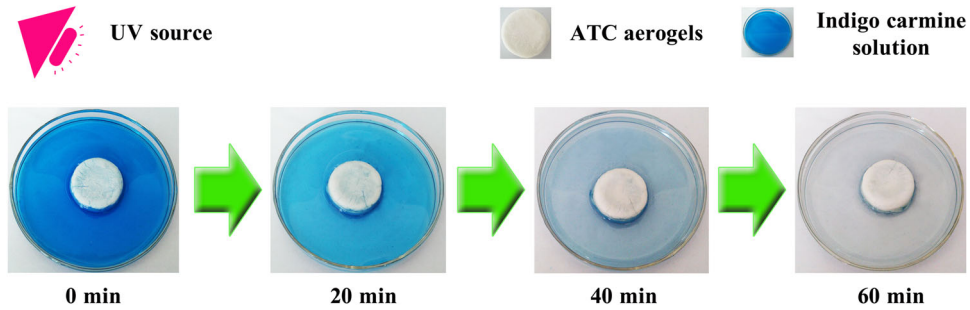

Fig. 7 Photocatalytic activity of ATC aerogels for indigo carmine dye degradation

1.3 cm^3 g^{-1} for PC aerogels and ATC aerogels, respectively. From these data, it was observed that specific surface area and pore volume of ATC aerogels were 8.6 and 30.0 % higher than those of PC aerogels, which indicated that the incorporation of TiO_2 particles into porous cellulose aerogels dramatically improved the pore characteristics.

Figure 6 showed the TG and DTG curves of ATC aerogels, which were recorded under a nitrogen atmosphere. For comparative purposes, the TG and DTG curves of PC aerogels were also displayed and exhibited only a strong exothermic peak at around 364 °C (Fig. 6b) corresponding to the thermal degradation of cellulose [41]. For the DTG curve of ATC aerogels, two exothermic peaks appeared during the whole pyrolysis process. The peak at around 297 °C was primarily due to decomposition and oxidation of residual organic substances during the preparation process [42]. In addition, the peak that was induced by cellulose pyrolysis occurred at around 353 °C for ATC aerogels, 11 °C lower than that of PC aerogels. The degradation in thermal stability of the composites might be due to the catalytic character of TiO_2, the loosening of molecular chains in crystalline regions of cellulose resulted from infusion of TiO_2 particles during the impregnation process, and the damage of cellulose chains caused by a small amount of HNO_3 in the sol [43, 44]. In addition, the residual char yields above 800 °C were 4.3 % for PC aerogels and 22.0 % for ATC aerogels, respectively. Owing to the high decomposition temperature of TiO_2 (>1000 °C), the content of TiO_2 was almost not changed during the pyrolysis, indicating that the TiO_2 loading content in cellulose aerogels was approximately 17.7 %.

To investigate the potential photocatalytic ability of ATC aerogels, a simple photocatalytic degradation test of indigo carmine dye was implemented under UV light for approximately 1 h (Fig. 7). For eliminating interference from adsorption effect of the sample, before the irradiation process, the aerogels sample was immersed in the indigo carmine solution and stirred for about 0.5 h to reach adsorption equilibrium. The color of the aerogels was transformed from white to nattier blue; however, the color of the solution still kept deep blue, which indicated that the absorption action of the porous aerogels did not significantly affect the solution color. In addition, during the UV illumination process, apparently, the drastic color changes did occur to the indigo carmine solution, which was gradually transformed from dark blue to transparent colorless with the prolongation of time. The results revealed some promising photocatalytic applications of ATC aerogels like treatment of organic dye wastewater. Meanwhile, the aerogels sample maintained the well-defined shape without any collapse throughout the entire UV radiation process, which provided convenience for recovery processing of the aerogels.

4 Conclusion

In this study, a simple facile room-temperature impregnation treatment of the cellulose hydrogels (the precursor of cellulose aerogels) in an anatase TiO_2 nanosol was carried out to complete the embedment of anatase titania into the porous structures. Meanwhile, the preparation of the cellulose hydrogels was based on a green cost-effective and low-pollution cellulose solvent named NaOH/PEG solution. After the freeze-drying process, the resulting hybrid ATC aerogels exhibited that the TiO_2 nanoparticles with diameters of 3.69 ± 0.77 nm were inserted into the cross-linked 3D networks. Moreover, the hybrid aerogels had improved specific surface area of around 201 $m^2\ g^{-1}$ and pore volume of approximately 1.3 $cm^3\ g^{-1}$, 8.6 and 30.0 % higher than those of PC aerogels (185 $m^2\ g^{-1}$ and 1.0 $cm^3\ g^{-1}$). But the additional handlings including impregnation and subsequent heating treatments lowered the thermal stability of ATC aerogels, because of the shift of the characteristic exothermic peaks to lower temperatures. In addition, ATC aerogels also showed a high photocatalytic activity for the indigo carmine dye degradation under UV light and maintained the well-defined shape throughout the entire radiation process, which indicated some potential applications in water purification, air cleaning, and chemical leaks.

Acknowledgments This work was financially supported by the National Natural Science Foundation of China (Grant Nos. 31270590 and 31470584).

References

1. Y. Chujo, Curr. Opin. Solid State Mater. **1**, 806 (1996)
2. P. Kumar, V.V. Guliants, Microporous Mesoporous Mater. **132**, 1 (2010)
3. V. Dufaud, M.E. Davis, J. Am. Chem. Soc. **125**, 9403 (2003)
4. B.C. Steele, A. Heinzel, Nature **414**, 345 (2001)
5. R.P. Swatloski, S.K. Spear, J.D. Holbrey, R.D. Rogers, J. Am. Chem. Soc. **124**, 4974 (2002)
6. T. Dawsey, C.L. McCormick, Macromolecules **30**, 405 (1990)
7. M.W. Frey, J.A. Cuculo, S.A. Khan, J. Polym. Sci. Polym. Phys. **34**, 2375 (1996)
8. H. Qi, C. Chang, L. Zhang, Cellulose **15**, 779 (2008)
9. L. Yan, Z. Gao, Cellulose **15**, 789 (2008)
10. J.T. Korhonen, M. Kettunen, R.H. Ras, O. Ikkala, ACS Appl. Mater. Interaces **3**, 1813 (2011)
11. G. Siqueira, J. Bras, A. Dufresne, Polymer **2**, 728 (2010)
12. G. Zheng, Y. Cui, E. Karabulut, L. Wågberg, H. Zhu, L. Hu, MRS Bull. **38**, 320 (2013)
13. J. Cai, S. Kimura, M. Wada, S. Kuga, Biomacromolecules **10**, 87 (2008)
14. J. Zhang, Y. Cao, J. Feng, P. Wu, J. Phys. Chem. C **116**, 8063 (2012)
15. C. Wan, Y. Jiao, Q. Sun, J. Li, Polym. Compos. (2014). doi:10.1002/pc.23276
16. R.T. Olsson, M.A. Samir, G. Salazar-Alvarez, L. Belova, V. Ström, L.A. Berglund, O. Ikkala, J. Nogues, U.W. Gedde, Nat. Nanotechnol. **5**, 584 (2010)
17. U. Diebold, Appl. Phys. A **76**, 681 (2003)
18. D. Dambournet, I. Belharouak, K. Amine, Chem. Mater. **22**, 1173 (2009)
19. T. Peng, D. Zhao, K. Dai, W. Shi, K. Hirao, J. Phys. Chem. B **109**, 4947 (2005)
20. K. Woan, G. Pyrgiotakis, W. Sigmund, Adv. Mater. **21**, 2233 (2009)
21. A.R. Khataee, G.A. Mansoori, *Nanostructured Titanium Dioxide Materials: Properties, Preparation and Applications* (World Scientific Publishing Co., Singapore, 2011)
22. B.L. Bischoff, M.A. Anderson, Chem. Mater. **7**, 1772 (1995)
23. S.C. Pillai, P. Periyat, R. George, D.E. McCormack, M.K. Seery, H. Hayden, J. Colreavy, D. Corr, S.J. Hinder, J. Phys. Chem. C **111**, 1605 (2007)
24. J.-N. Nian, H. Teng, J. Phys. Chem. B **110**, 4193 (2006)
25. G. Boschloo, A. Goossens, J. Schoonman, J. Electrochem. Soc. **144**, 1311 (1997)
26. J. Sun, L. Gao, Q. Zhang, J. Am. Ceram. Soc. **10**, 1677 (2003)
27. J. Li, C. Wan, Y. Lu, Q. Sun, Front. Agric. Sci. Eng. **1**, 46 (2014)
28. D. Wu, M. Long, J. Zhou, W. Cai, X. Zhu, C. Chen, Y. Wu, Surf. Coat. Technol. **203**, 3728 (2009)
29. P. Tingaut, T. Zimmermann, G. Sèbe, J. Mater. Chem. **22**, 20105 (2012)
30. T. Kashiwagi, F. Du, K.I. Winey, K.M. Groth, J.R. Shields, S.P. Bellayer, H. Kim, J.F. Douglas, Polymer **46**, 471 (2005)
31. J. Jordan, K.I. Jacob, R. Tannenbaum, M.A. Sharaf, I. Jasiuk, Mater. Sci. Eng. A **393**, 1 (2005)
32. B. Liu, A. Khare, E.S. Aydil, Chem. Commun. **48**, 8565 (2012)
33. Y. Jiang, D. Yang, L. Zhang, Q. Sun, X. Sun, J. Li, Z. Jiang, Adv. Funct. Mater. **19**, 150 (2009)
34. B. Erdem, R.A. Hunsicker, G.W. Simmons, E.D. Sudol, V.L. Dimonie, M.S. El-Aasser, Langmuir **17**, 2664 (2001)
35. W.-J. Gong, H.-W. Tao, G.-L. Zi, X.-Y. Yang, Y.-L. Yan, B. Li, J.-Q. Wang, Res. Chem. Intermed. **35**, 751 (2009)
36. G.T.S. How, A. Pandikumar, H.N. Ming, L.H. Ngee, Scientific Reports-UK **4** (2014)
37. P. Wen, H. Itoh, W. Tang, Q. Feng, Langmuir **23**, 11782 (2007)
38. Y. Nishiyama, P. Langan, H. Chanzy, J. Am. Chem. Soc. **124**, 9074 (2002)
39. H. Sehaqui, Q. Zhou, L.A. Berglund, Compos. Sci. Technol. **71**, 1593 (2011)
40. T.Y. Wei, C.Y. Kuo, Y.J. Hsu, S.Y. Lu, Y.C. Chang, Microporous Mesoporous Mater. **112**, 580 (2008)
41. R. Baker, J. Therm. Anal. Calorim. **8**, 163 (1975)
42. A. Tang, Y. Deng, J. Jin, H. Yang, Sci World J. **2012** (2012). doi:10.1100/2012/480527
43. Q. Yu, P. Wu, P. Xu, L. Li, T. Liu, L. Zhao, Green Chem. **10**, 1061 (2008)
44. H. Wang, W. Zhong, P. Xu, Q. Du, Compos. Part A Appl. Sci. **36**, 909 (2005)